Crystal Structure of Fructose-1,6-bisphosphate Aldolase from the Human Malaria Parasite *Plasmodium falciparum*[†,▽]

Hidong Kim,[‡,§] Ulrich Certa,[∥] Heinz Döbeli,[∥] Peter Jakob,[∥] and Wim G. J. Hol*[,‡,⊥]

Howard Hughes Medical Institute and Departments of Biological Structure and Biochemistry, Biomolecular Structure Center, Box 357742, University of Washington, Seattle, Washington 98195, and Department PRT, F. Hoffmann-La Roche, Ltd., Basel, Switzerland

Received September 8, 1997

ABSTRACT: The structure of the glycolytic enzyme class I fructose-1,6-bisphosphate aldolase from the human malaria parasite *Plasmodium falciparum* has been determined by X-ray crystallography. Homotetrameric *P. falciparum* aldolase (PfALDO) crystallizes in space group $P3_221$ with one 80 kDa dimer per asymmetric unit. The final refined PfALDO model has an *R*-factor of 0.239 and an *R*-free of 0.329 with respect to data from 8 to 3.0 Å resolution. PfALDO is potentially a target for antimalarial drug design as the intraerythrocytic merozoite lifestage of *P. falciparum* is completely dependent upon glycolysis for its ATP production. Thus, inhibitors directed against the glycolytic enzymes in *P. falciparum* may be effective in killing the parasite. The structure of PfALDO is compared with the previously determined structure of human aldolase in order to determine possible targets for the structure-based design of selective PfALDO ligands. The salient structural differences include a hydrophobic pocket on the surface of PfALDO, which results from some amino acid changes and a single residue deletion compared with human aldolase, and the overall quaternary structure of the PfALDO tetramer, which buries less surface area than human aldolase.

Malaria is one of the world's most serious parasitic diseases, accounting for 300 to 500 million cases, and between 1.5 and 2.7 million deaths every year (*1*). This heavy toll on human life and health reflects the need for more effective antimalarial therapies, especially considering the rapid rise of resistance to currently available drugs in many strains of the parasite (*1*). The causative agent of malaria in humans, *Plasmodium falciparum*, undergoes a complex life cycle, both in the *Anopheles* mosquito vector and the human host. In the human host, it is the intraerythrocytic merozoite life stage of *P. falciparum* that is responsible for the characteristic chills, fever, and nausea symptoms of malaria paroxysm. This life stage of the parasite is peculiar in that, like the human erythrocyte, it lacks a functional tricarboxylic acid cycle and, therefore, depends entirely upon glycolysis for its ATP production (*2*). Thus, it is expected that selective inhibitors of *P. falciparum* glycolytic enzymes should kill the parasite (*3*).

The 10 enzymes of the glycolytic pathway that convert glucose 6-phosphate to pyruvate have been extensively studied, and the three-dimensional X-ray crystal structures of all of the glycolytic enzymes from various sources have been determined (*4*, *5*). Among the glycolytic enzymes, class I fructose-1,6-bisphosphate aldolase (ALDO)[1] is a homotetrameric enzyme with 222 molecular symmetry of total molecular weight 160 kDa. In the glycolytic pathway, aldolase catalyzes the aldol cleavage of fructose 1,6-bisphosphate (FBP) to dihydroxyacetone phosphate (DHAP) and glyceraldehyde 3-phosphate (GAP). In addition to FBP, fructose 1-phosphate (F1P) can also be a substrate in the aldol cleavage reaction.

In mammals, there are three aldolase isozymes: A, B, and C. These three isozymes are distinguished by different substrate specificities. The ratios of FBP:F1P cleavage rates are 50, 1, and 2, respectively, for the A, B, and C isozymes of rabbit aldolase (*6*). The three mammalian aldolase isozymes are also localized in different tissues. Isozyme A is present in virtually all tissues, but most notably in muscle. Isozyme A is also the aldolase isozyme in erythrocytes (*7*). Isozyme B is confined to the liver, kidney, and intestines, while isozyme C is found in brain and nerve tissues (*6*).

The X-ray crystal structures of *Drosophila melanogaster* aldolase (*8*), rabbit aldolase A (*9*), and human aldolase A (*10, 11*) have previously been reported. We have now determined the X-ray crystal structure of *P. falciparum* aldolase (PfALDO). The present structure of PfALDO allows a comparison between the previously determined aldolases and the malarial aldolase. Such analyses will be

[†] This research was supported in part by a major equipment grant from the Murdock Charitable Trust.

[▽] Brookhaven Protein Data Bank accession code 1A5C.

* To whom correspondence should be addressed.

[‡] Howard Hughes Medical Institute and Department of Biological Structure, University of Washington.

[§] Present address: Emerald BioStructures, Inc., 7865 NE Day Rd. W, Bainbridge Island, WA 98110.

[∥] Hoffmann-La Roche.

[⊥] Department of Biochemistry, University of Washington.

[1] Abbreviations: ALDO, fructose-1,6-bisphosphate aldolase; PfALDO, *Plasmodium falciparum* fructose-1,6-bisphosphate aldolase; hALDO, human fructose-1,6-bisphosphate aldolase; DmALDO, *Drosophila melanogaster* fructose-1,6-bisphosphate aldolase; FBP, fructose 1,6-bisphosphate; GAP, glyceraldehyde 3-phosphate; F1P, fructose 1-phosphate.

S0006-2960(97)02233-2 CCC: $15.00
Published on Web 03/13/1998

Table 1: X-Ray Data Statistics

data set	detector	res. (Å)	total refl.	unique refl.	completeness (%)	R_{merge}	$\langle I/\sigma \rangle$	R_{merge} (last shell)	$\langle I/\sigma \rangle$ (last shell)
lab I	R-AXIS II	3.7	84 491	11 995	97	0.235	5.0	0.643 (3.83-3.70)	1.6
lab II	R-AXIS II	3.5	102 404	13 959	99	0.163	8.1	0.480 (3.63-3.50)	2.4
SSRL	SSRL 1-5	3.4	89 436	13 681	89	0.136	6.2	0.452 (3.52-3.40)	2.0
merged	lab II + SSRL	3.4	204 695	15 248	99	0.196	12.8	0.627 (3.52-3.40)	3.9
ESRF	ESRF BM2	3.0	65 931	20 677	94	0.077	8.2	0.175 (3.08-3.00)	3.4

the first phase in the structure-based design of novel selective inhibitors of PfALDO, which may serve as antimalarial drug leads.

MATERIALS AND METHODS

Preparation and Purification of P. falciparum Aldolase. Cloning, expression, and fermentation in *Escherichia coli* of recombinant PfALDO was performed according to a previously reported procedure (*12*). The His affinity tag was subsequently deleted from the recombinant PfALDO. Consequently, the purification protocol was modified from the previous report in the following manner.

PfALDO-overexpressing *E. coli* cells (50 g) were suspended in 50 mM Tris-HCl/5 mM EDTA/1 mM *o*-phenanthroline/0.1% NaN_3/pH 6 and lysed by ultrasonication. The lysate was centrifuged, and the supernatant was clarified by filtration. Six subsequent column chromatography steps were performed on a BioCAD perfusion chromatography workstation. (Step 1) The clarified cell lysate was purified by cation exchange chromatography using Macroprep HS 50 resin (Bio-Rad) in a 1.6 cm × 0.5 cm bed volume at a flow rate of 30 mL/min. The sample was loaded with 50 mM Tris-HCl/5 mM EDTA/0.1% NaN_3/pH 6. PfALDO was eluted with a [NaCl] gradient. The peak fractions were pooled and made 1 M in $(NH_4)_2SO_4$. (Step 2) The $(NH_4)_2SO_4$ pool was purified by hydrophobic interaction chromatography using Source 15 PHE resin (Pharmacia) in a 3.5 cm × 5.2 cm bed volume at a flow rate of 30 mL/min. The sample was loaded with 50 mM Na_2HPO_4/1 M $(NH_4)_2SO_4$/5 mM EDTA/0.1% NaN_3/pH 6. Fractions containing PfALDO were eluted with 25 mM Na_2HPO_4/5 mM EDTA/0.1% NaN_3/pH 8. (Step 3) The pooled fractions containing PfALDO were desalted over Sephadex G25 SF resin (Pharmacia) in a bed volume of 2.6 cm × 5.6 cm. The buffer was 25 mM Na_2HPO_4/pH 8. (Step 4) The desalted sample was purified by anion-exchange chromatography using Poros 20HQ resin (PerSeptive) in a 0.46 cm × 10 cm bed volume at a flow rate of 20 mL/min. The sample was loaded with 25 mM Na_2HPO_4/0.1% NaN_3/pH 6. Fractions containing PfALDO do not bind to the column under these conditions. (Step 5) The flowthrough fraction was purified by cation-exchange chromatography using Poros 20HS resin (PerSeptive) in a bed volume of 0.46 cm × 10 cm at a flow rate of 20 mL/min. The sample was loaded with 25 mM Na_2HPO_4/0.1% NaN_3/pH 6. PfALDO was eluted with a [NaCl] gradient. Fifteen milligrams of PfALDO was recovered at this point. (Step 6) PfALDO was further purified by size-exclusion chromatography using Superdex 200 resin (Pharmacia) in a 1.6 cm × 60 cm bed volume. The elution buffer was 25 mM Na_2HPO_4/0.1% NaN_3/pH6. Ten milligrams of pure PfALDO was recovered from this column. Prior to crystallization, the PfALDO was dialyzed against 0.1 M TEA/50 mM NaCl/1 mM DTT/1 mM EDTA/pH 7.6 and concentrated to 6 mg/mL protein.

Edman degradation of the purified PfALDO revealed the N-terminal sequence AHCTEYMNAPK. This sequence is identical to the N-terminal sequence of the natural PfALDO, except for the presence of the N-terminal acetyl group in the natural PfALDO (*13*). The specific activity of the purified PfALDO with respect to fructose 1,6-bisphosphate cleavage is 7 units/mg, and the K_m is 10 μM. The specific activity and K_m of the His-tagged PfALDO are 4 units/mg and 10 μM, respectively (*12*).

Crystallization and X-ray Diffraction Data Collection. Crystals of PfALDO were grown by hanging drop vapor diffusion against a reservoir solution of 2.0 M $(NH_4)_2SO_4$/5% 2-propanol. Cubelike crystals up to 100 μm in dimension appeared within 3 weeks. (Initial crystallization trials with the His affinity-tagged PfALDO (*12*) were unsuccessful.) The space group of the crystals was $P3_221$, with unit cell parameters $a = 119.2$ Å, $c = 132.3$ Å, and 1 PfALDO dimer/asymmetric unit.

X-ray diffraction data were collected using laboratory equipment and synchrotron radiation at the Stanford Synchrotron Radiation Laboratory (SSRL) and also at the European Synchrotron Radiation Facility (ESRF) (Table 1). All data were collected at −160 °C. The cryoprotectant was a 1:1 mixture of crystallization solution and glycerol. Before transfer to the cryoprotectant, the crystals were first cross-linked by soaking in a solution of 0.1% glutaraldehyde in the crystallization solution for 15 min. Laboratory and SSRL data were processed using DENZO and SCALEPACK (*14*). ESRF data were processed using XDS (*15*−*17*).

Structure Determination and Model Refinement. The initial structure of PfALDO was obtained by molecular replacement from the 3.7 Å laboratory data set (Table 1). The search model for molecular replacement was the 55% sequence-identical structure of the *Drosophila melanogaster* aldolase (DmALDO) tetramer (*8*). The cross-rotation function was calculated with ALMN (*18*) using data from 8 to 5.0 Å and a Patterson radius of 30 Å. The search resulted in a 5σ peak for the rotation $\alpha = 81.4°$, $\beta = 42.2°$, and $\gamma = 6.0°$ (Crowther Eulerian angles), which was the highest peak in the search.

After the tetrameric model was oriented according to the cross-rotation solution, the translation function was run with TFFC (*18*) in space groups $P321$, $P3_121$, and $P3_221$. The search in $P3_221$ gave a single clear 20σ peak, while the translation functions in $P321$ and $P3_121$ resulted in only 10σ peaks. The *R*-factor (*R*-factor $= \sum_{hkl}||F_o| - |F_c||/|F_o|$) of this molecular replacement solution was 0.475 for data from 8 to 5.0 Å. Analysis of the packing showed that one of the molecular 2-fold axes was coincident with a crystallographic 2-fold axis, clearly indicating that the content of the asymmetric unit was a dimer and not the entire tetramer.

Model building and refinement was begun using a merged 3.4 Å data set which consisted of laboratory and synchrotron

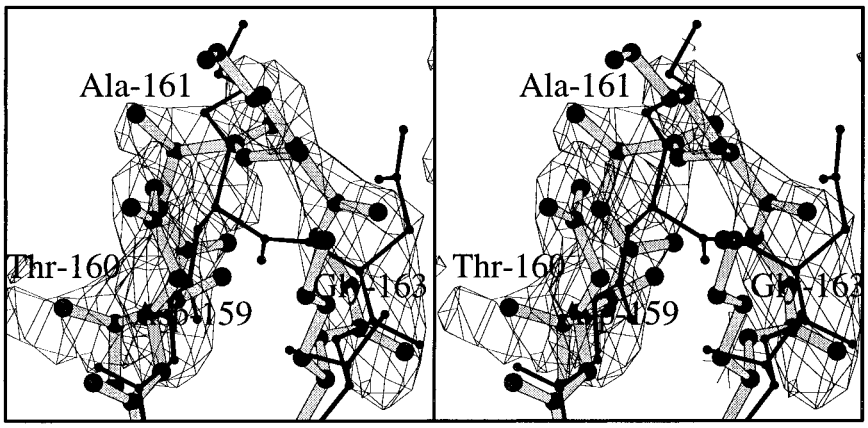

DmALDO 152KIG--KNT157
PfALDO 157VIDTAKGK164

FIGURE 1: Comparison of the loop containing Ala-161 in PfALDO and the structurally corresponding loop in DmALDO. (Left) Stereoview of SIGMAA-weighted omit $F_o - F_c$ map of PfALDO. Residues Asp-159−Gly-163 (PfALDO numbering) were omitted from the F_c calculation. The map was calculated using the "merged" data set (Table 1). The *R*-factor of the model was 0.289. The contour level is 1.5σ. The final refined model of PfALDO and the structure of DmALDO are superimposed. PfALDO is drawn with thick, lightly shaded bonds. DmALDO is drawn with thin, darkly shaded bonds. (Right) Sequence alignment of the loops. Residue numberings are indicated for each sequence. Dashes in the DmALDO sequence indicate amino acid deletions. The figure was made with MOLSCRIPT (*44*) and MINIMAGE (*45*).

Table 2: PfALDO Refinement Statistics

space group	$P3_221$
unit cell	$a = 119.2$ Å, $c = 132.3$ Å
asymmetric unit	80 kDa dimer
resolution range	8.0-3.0 Å
R_{factor}	0.239
R_{free}	0.329
bond length deviation	0.007 Å
bond angle deviation	1.3°
average *B*	29 Å^2

data (the "merged" set in Table 1). The starting point for refinement was a multi-Ala dimer model that contained all side chains conserved between PfALDO and DmALDO. The PfALDO model was completed by building into SIGMAA-weighted (*19*) $2F_o - F_c$ and 2-fold noncrystallographic symmetry-averaged electron density maps. Density modification was executed with DM (*20*). Partial models were then refined by positional refinement and simulated annealing against data from 8 to 3.4 Å. Despite the rather weak data, the electron density maps clearly showed features characteristic of PfALDO (Figure 1).

The 3.0 Å ESRF data set (Table 1) was used for the final refinement of the PfALDO model, which included grouped *B*-factor refinement in which there were two *B*-factor groups for each residue, one for backbone and one for side-chain atoms. The *R*-factor of the final PfALDO model is 0.239. A 5% test data set was used to monitor *R*-free throughout the refinement. The *R*-free dropped during every stage of the refinement, and the *R*-free of the final model is 0.329 (Table 2).

The final refined PfALDO model contains a single polypeptide chain spanning residues Leu-13 through Gly-354 of the PfALDO sequence for each monomer of the dimer. No waters were incorporated into the model. The Ramachandran plot shows no residues with disallowed dihedral angles (Figure 2). All model refinements were executed with X-PLOR (*21*). X-PLOR was also used to calculate accessible surface area with a probe of radius 1.6 Å. All model building was done with O (*22*).

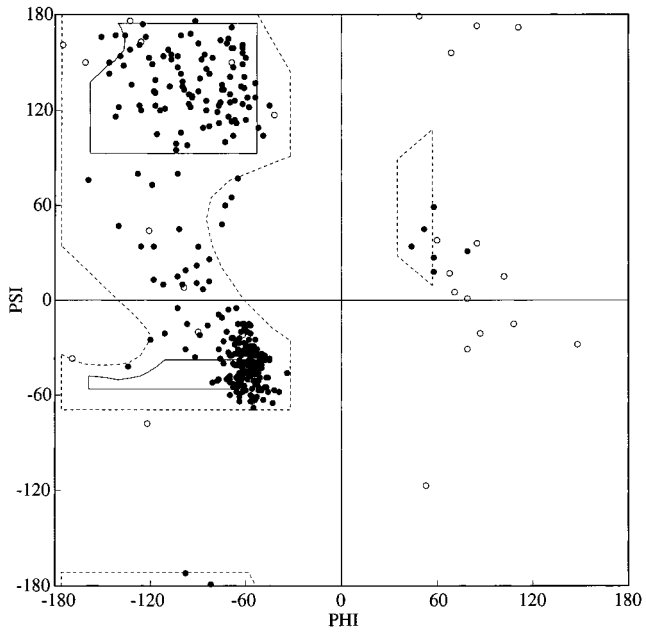

FIGURE 2: Ramachandran plot of the final refined PfALDO subunit. Glycines are indicated by unfilled circles.

RESULTS AND DISCUSSION

Quality of the Structure. The overall fold of the PfALDO monomer is an $(\alpha/\beta)_8$ barrel as seen in the previous structures of class I aldolase from rabbit, human, and *D. melanogaster* (*8*, *9*, *11*) (Figure 3). As tight noncrystallographic symmetry restraints were imposed on the dimer model during refinement, the two crystallographically independent PfALDO monomers are virtually identical, with the rms deviation between their C^αs being <0.2 Å after superposition.

Although the resolution of the present PfALDO structure is not as high as those of previous aldolase structures, there are several indications that vouch for the correctness of the structure. First of all, the stereochemical correctness of the PfALDO structure is confirmed by the Ramachandran plot (Figure 2). According to recent Ramachandran criteria derived from an analysis of high-resolution protein structures (*23*), only 13 of 311 non-Gly residues in the PfALDO monomer fall outside of the 98% $\phi-\psi$ regions. Furthermore,

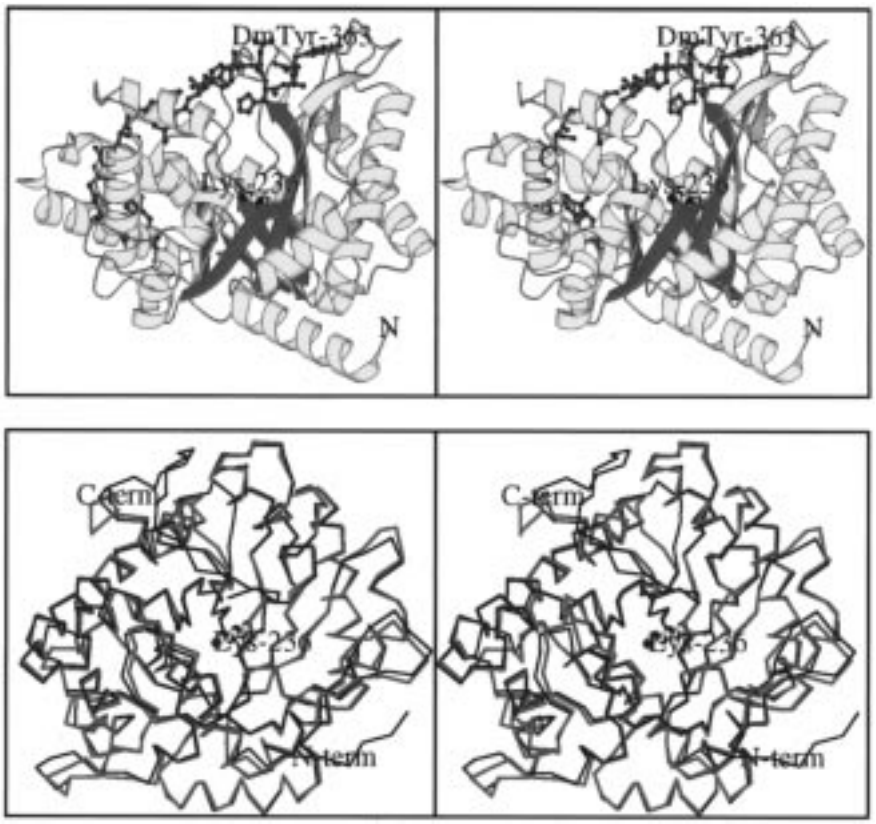

FIGURE 3: Tertiary structure of PfALDO. (a, top) Ribbon diagram of the PfALDO monomer viewed approximately perpendicular to the axis of the central β-barrel. The central β-barrel is drawn in green. The C-terminal tail of DmALDO is shown in cyan ball-and-stick representation after superposition of the DmALDO monomer onto the PfALDO monomer to show a possible conformation of the PfALDO C-terminal tail, which was not visible in the electron density maps. The C-terminal Tyr-363 of DmALDO is labeled. The catalytic Lys-236 is shown in ball-and-stick representation. The N-terminal Leu-13 and the C-terminal Gly-354 of the PfALDO model are also labeled. (b, bottom) Stereoview of the superposition of C^{α} traces of PfALDO and hALDO-A viewed approximately along the axis of the central β-barrel. PfALDO is drawn in thick red lines and hALDO-A in thin black lines after superposition onto PfALDO. The catalytic Lys-236 of PfALDO is shown in ball-and-stick representation. The figure was made with MOLSCRIPT.

the rms deviations from ideality for bond length and bond angle are 0.007 Å and 1.3°, respectively.

Other indications of the correctness of the PfALDO structure are seen in the electron density maps, which at various stages in the model building process confirmed characteristic features of PfALDO. One such example is the 160s loop in PfALDO. At an *R*-factor of 0.289, SIGMAA-weighted omit $F_o - F_c$ maps clearly showed the Thr-Ala insertion between Asp-159 and Lys-162, compared with the DmALDO sequence (Figure 1).

There is also the important deletion of Leu-291 from the DmALDO sequence in PfALDO (Figure 4). This is manifested in part by the backbone of the loop spanning Leu-296−Pro-300 in PfALDO deviating by nearly 6 Å from the conformations of the corresponding loops in both DmALDO and hALDO-A, both of whose sequences conserve Leu-291. The conformation of this loop in PfALDO is confirmed by SIGMAA-weighted omit $F_o - F_c$ maps (not shown).

Comparison with Other Aldolases. Overall, there is a high degree of structural similarity between PfALDO and other aldolases (Figure 3). For the monomers, the rms deviation in C^{α} positions after superposition is 1.2 Å between PfALDO and hALDO-A and 1.4 Å between PfALDO and DmALDO. For these comparisons, the 14 C-terminal residues of the flexible C-terminal tails in hALDO-A and DmALDO were removed. The structural similarities between PfALDO and the previously determined aldolases also extend to their quaternary structures. The rms deviation in C^{α} positions after superposition of tetramers is 1.4 Å between PfALDO and hALDO-A and 1.5 Å between PfALDO and DmALDO. These structural similarities are expected from the sequence identities among the aldolases, which are 55% between PfALDO and DmALDO, and 54% between PfALDO and hALDO-A (Table 3).

In the 222 symmetric aldolase tetramer, there are three different types of dimers. These dimers have varying degrees of buried surface area. In PfALDO, hALDO-A, and DmALDO, the AB and AD dimers bury the most surface area, while there is relatively little intermolecular contact in the AC dimer. For the present PfALDO structure, the buried surface area for each of the three dimers is as follows: AB, 2200 $Å^2$; AC, 210 $Å^2$; and AD, 1600 $Å^2$. For hALDO-A, the buried surface for each of the three dimers is as follows: AB, 2900 $Å^2$; AC, 360 $Å^2$; and AD, 2800 $Å^2$. hALDO-A appears to be a more tightly associated tetramer than PfALDO. This tighter association for the hALDO-A tetramer is most pronounced in the AD dimer interface. In the PfALDO structure, the asymmetric unit of the crystal contains the AB dimer, which buries the most surface area.

One of the regions of greatest similarity among aldolases, in both three-dimensional structure and amino acid sequence, is the active site. The catalytic mechanism of class I aldolase proceeds through a Schiff base intermediate, which is a covalent adduct formed by the nucleophilic attack of the N^{ζ}

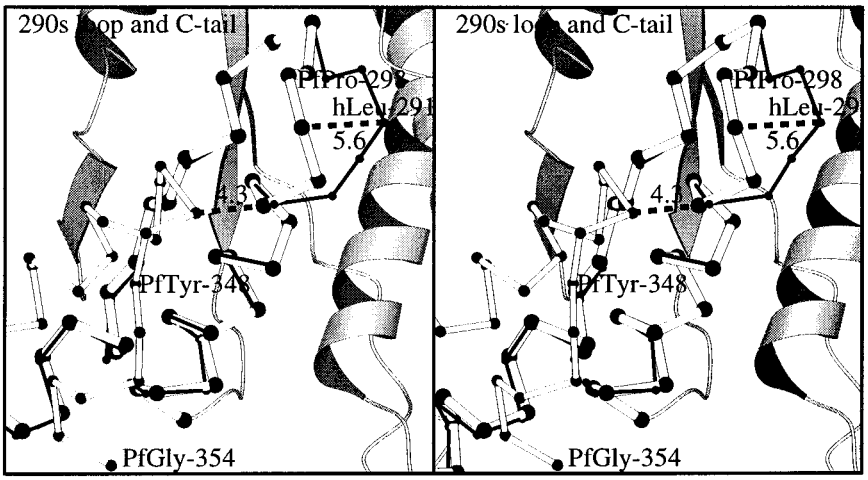

P. falcip.	294NALG-PHPW301
human A	287.KCPLLK..295
human B	287.LCPL.K..295
human C	287.RCPL.R..295
rat A	287.KCPLLK..295
rabbit A	287.KCPLLK..295
D. melano.	287.NVPLIR..295
T. brucei	287.NCPL.R..295

FIGURE 4: Comparison of the 290s loop regions in various aldolases. (Left) Stereoview of 290s loop regions in PfALDO and hALDO-A. The C^{α} trace of the 290s loop, and the α-helix preceding the C-terminal tail in PfALDO are drawn with open bonds. PfALDO secondary structures are drawn as gray ribbons. The backbone of the 290s loop region in hALDO-A after superposition is drawn with solid bonds. The distances between the 290s loops in PfALDO and hALDO-A, and the distances between the 290s loop and the beginning of the C-terminal tail in PfALDO are indicated in angstroms. The figure was made with MOLSCRIPT. (Right) Sequence alignment of 290s loop regions in various aldolases. A dot indicates that the residue is conserved with the PfALDO sequence. A dash indicates a deletion. Residue numbers are indicated for each sequence.

Table 3: Aldolase Sequence Identities[a]

	human A	human B	human C	PfALDO
human A		69	82	54
human B	69		70	51
human C	82	70		57
PfALDO	54	51	57	

[a] Identities are given as percentages.

of a critical lysine on the C2 carbonyl of FBP. (For a review of class I aldolase, see ref *24*.) All of the residues that have previously been implicated in the catalytic mechanism of aldolase are present in PfALDO. In addition to the nucleophilic Schiff base-forming Lys-236, there are also Lys-47, Arg-48, Lys-151, and Arg-309, which have been proposed to bind the phosphates of FBP (*11*).

Recently, the crystal structure of rabbit muscle aldolase complexed with DHAP, the product of FBP cleavage, has been reported (*25*). In this study, the aldolase−DHAP complex crystallized with an entire aldolase tetramer per asymmetric unit. DHAP was found to bind in the active site of rabbit muscle aldolase in three distinct binding modes. The residues that bind DHAP in rabbit muscle aldolase are entirely conserved in PfALDO. These residues in PfALDO include Asp-39, Arg-48, Glu-195, Ser-278, and Arg-309.

While the amino acid sequence and the three-dimensional structure of the PfALDO active site appear to be well-conserved among aldolases (*8, 9, 11*), other regions of the PfALDO structure diverge from previous aldolase structures. There are some regions where the backbone of PfALDO deviates by almost 6 Å from the backbones of DmALDO and hALDO-A after superposition. These generally occur at surface loops, away from the active site.

One of the potentially most interesting regions of structural diversity among aldolases is the C-terminal tail. This region also shows great sequence diversity between species, although the C-terminal Tyr is strictly conserved (Figure 5). The importance of the C-terminal Tyr in the aldolase-catalyzed reaction has been demonstrated by carboxypeptidase digests of aldolase. Removal of the C-terminal Tyr by carboxypeptidase treatment reduces the activity of aldolase by nearly 2 orders of magnitude with respect to cleavage of FBP (*26*, *27*). The DmALDO structure showed the C-terminal tail to drape over the active-site cleft, while the C-terminal tail in the hALDO-A structure burrows into the active site (*8*, *11*). In both DmALDO and hALDO-A, access to the active site is partially occluded by the conformation of the C-terminal tail. It appears that the C-terminal tail must undergo a large motion during catalysis to allow the entry and release of substrates and products. Thus, the catalytic importance of the C-terminal tail and its great sequence diversity among species makes this region of aldolase an attractive target for specific inhibitor design.

The C-terminal tail, unfortunately, has generally been the least well-defined region in aldolase crystal structures. The initial determination of the rabbit aldolase structure at 2.7 Å resolution was not able to definitively place the 18 C-terminal residues (*9*). The more recent, higher resolution structure of the rabbit aldolase−DHAP complex, which crystallized with one tetramer per asymmetric unit, showed the conformation of the C-terminal tail to be very sensitive to ligand binding (*25*). In the current PfALDO structure, the C-terminal 14 residues could not be fully traced. However, enough of the chain was sufficiently well-defined to indicate that the conformation of the C-terminal tail in PfALDO is more like that in DmALDO than in hALDO-A (Figure 5). In DmALDO, the C-terminal tail is in an extended conformation that hovers over the C-terminal end of the central β-barrel. In hALDO-A, the C-terminal tail takes a sharp turn away from the central β-barrel at Pro-344 and then doubles back toward the active site at Gly-349. In SIGMAA-weighted $F_o - F_c$ maps for which residues Tyr-348 and beyond in PfALDO were omitted from the F_c calculation, electron density is seen up through Gly-354. By sequence alignment, this residue corresponds to Ala-348 in DmALDO and Gly-349 in hALDO-A. The conformation of this portion of the C-terminal tail in PfALDO follows that seen in DmALDO and deviates greatly from the conformation observed in hALDO-A.

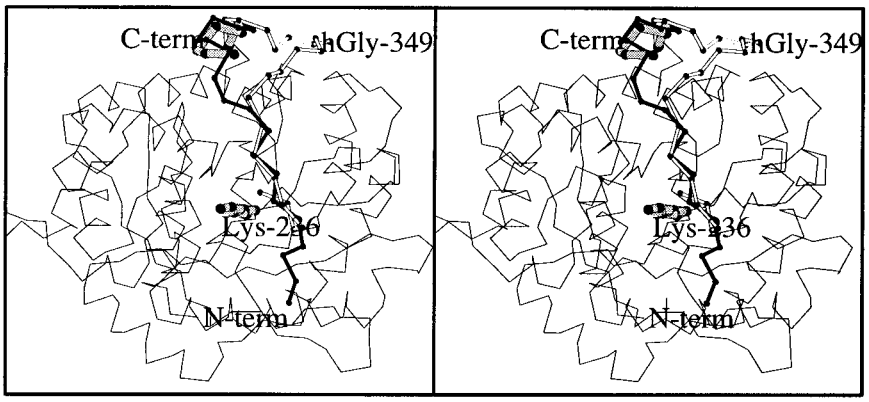

P. falcip.	351	GAGGENAGASLYEKKYVY 368
human A	346	.QA.AA.SE..FVSNHA. 363
human B	346	.SS.AASTQ..FTAC.T. 363
human C	346	.ED.GA.AQ...IANHA. 363
rat A	346	.QA.AA.SE..FISNHA. 363
rabbit A	346	.QA.AA.SE..FISNHA. 363
D. melano.	343	AGSAGAGSG..FVANHA. 360
T. brucei	354	R.DDDKDSQ...VAGNT. 371

FIGURE 5: Structure and sequence of aldolase C-terminal tails. (Left) Stereoview of superposition of aldolase C-terminal tails. The C-terminal tails of hALDO-A and DmALDO are shown after superposition of hALDO-A and DmALDO onto the PfALDO structure. The C-terminal tail of PfALDO is drawn with thick, lightly shaded bonds. The remainder of the PfALDO C^{α} secondary structure is drawn with thin lines. The hALDO-A C-terminal tail and the DmALDO C-terminal tail are drawn with open and solid bonds, respectively. The critical active-site Lys-236 of PfALDO is shown in ball-and-stick representation. hALDO-A Gly-349, which shows a deviation of 20 Å from PfALDO Gly-354, the corresponding sequence-aligned residue of PfALDO, is indicated to show the greatest deviation between the C-terminal tails of PfALDO and HALDO-A. The figure was made with MOLSCRIPT. (Right) Sequence alignment of C-terminal 18 residues in various aldolases. Residue numbers are indicated for each sequence. A dot indicates the same amino acid as in PfALDO.

Potential Targets for Structure-Based Drug Design in PfALDO. PfALDO is now the fourth malarial protein whose X-ray crystal structure has been determined, following the recent structure determinations of plasmepsin II (*28*), lactate dehydrogenase (*29*), and triosephosphate isomerase (*30*) from *P. falciparum*. The crystal structure of PfALDO may now be used for structure-based selective ligand design. As mentioned before, PfALDO appears to be an attractive target for structure-based drug design as the erythrocytic lifestage of *P. falciparum* is entirely dependent upon glycolysis for its ATP production (*2*, *3*). The energy requirement of the intraerythrocytic parasite is reflected in the enormous glucose consumption of infected erythrocytes, which is up to 30 times higher than that of normal erythrocytes (*2*, *31*). Thus, it is expected that selective inhibitors of the parasite glycolytic enzymes, of which PfALDO is one, will severely interfere with parasite function and kill the parasite.

The search for selective inhibitors of PfALDO that do not affect the human host aldolase promises to be challenging. The problem of designing selectivity is compounded by the presence of three different aldolase isozymes in humans. These three human aldolase isozymes are between 69% and 82% sequence identical among themselves, and PfALDO is a little more than 50% sequence identical with all three of the human isozymes (Table 3). If the highly variable C-terminal tail is excluded, it appears that the active site is one of the most highly conserved regions among PfALDO and the three human aldolases. The amino acid difference closest to the active site is Val-275 in PfALDO, equivalent to Thr-268 in hALDO-A, which occurs ~6 Å from the N^{ζ} of the critical lysine. This residue in both PfALDO and hALDO-A is virtually completely buried and so is unfortunately of little use for the design of selective inhibitors. Other amino acid changes in the vicinity of the active site are more conservative hydrophobic residue changes: Leu-28 in PfALDO going to Ile-22 in all three human aldolases, and Ala-81 in PfALDO instead of Val-76, also in all three human aldolases. These amino acid changes would seem to be quite challenging to exploit for designing selective ligands of the malarial aldolase.

A promising region of PfALDO to target for selectivity design appears to be the C-terminal tail. Even though the C-terminal tail of PfALDO could not be seen in the electron density maps, this region appears to be worth pursuing as a selectivity target due to the great sequence differences between PfALDO and the human aldolases (Figure 5). The sequence comparison reveals some very nonconservative amino acid changes between the C-terminal tails of PfALDO and hALDO-A, such as Glu-355 and Glu-363 in PfALDO, whose corresponding residues in hALDO-A are Ala and Val, respectively. An especially interesting sequence feature of the PfALDO C-terminal tail is the Lys-364-Lys-365 tandem, which appears to be a unique characteristic of malarial aldolases. This lysine tandem is also present in the two aldolase isozymes of the murine malaria parasite *Plasmodium berghei* (*32*). The two murine malaria aldolases are 99% and 87% sequence-identical with PfALDO. All known vertebrate aldolases lack such a tandem lysine repeat near the C-terminal tyrosine (*33*). This Lys-Lys tandem may be a good initial target for designing specific ligands of the PfALDO C-terminal tail, which might interfere with the proposed motion of the tail during catalysis.

A second interesting difference between the structures of PfALDO and hALDO-A that may be exploited for the design of selective lead compounds occurs at the 290s loop of PfALDO. Located near the beginning of the C-terminal tail, the 290s loop region in PfALDO contains an unusual amino acid sequence and a conformational change compared with other aldolases. The sequence of PfALDO in this region contains a deletion of a Leu that is conserved in most other aldolases, including all three human isozymes (Figure 4). There are also some prominent amino acid changes between PfALDO and hALDO-A in this region. Ala-295 and His-299 in PfALDO are both changed to Lys in the hALDO-A sequence. This single amino acid deletion and the amino acid substitutions result in a nearly 6 Å deviation of the backbone of the PfALDO 290s loop from the conformation of the corresponding loop in hALDO-A (Figure 4).

This 290s loop and the loops containing Ala-31 and Gly-346 define a binding pocket, which in PfALDO is topologi-

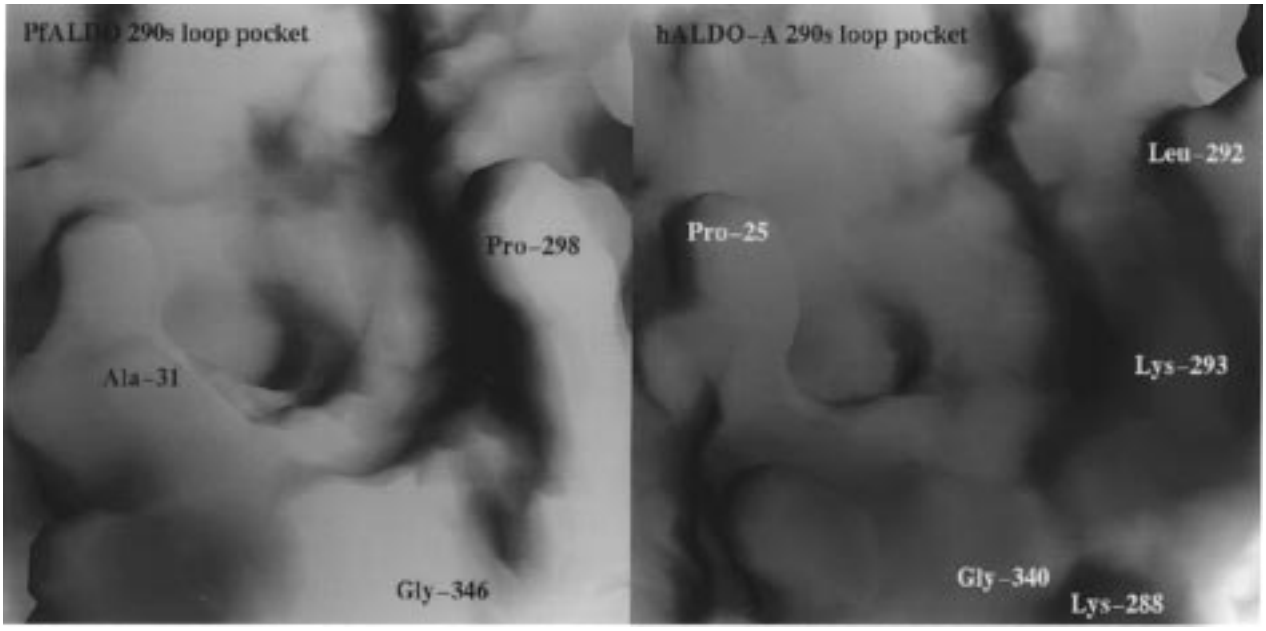

FIGURE 6: The 290s loop pocket in aldolase. Color-coded surface potentials are shown: white, hydrophobic; blue, basic; red, acidic. (a, left) The 290s loop pocket in PfALDO. Pro-298 of the 290s loop is indicated. (b, right) The 290s loop pocket in hALDO-A. Leu-292 of the 290s loop is indicated. Notice how access to the hydrophobic pocket in PfALDO appears more restricted due to Pro-298, whereas the corresponding region in hALDO-A is much more open and basic. The figure was made with GRASP (*46*).

cally and electrostatically significantly different from the corresponding pocket in hALDO-A. The amino acids in the 290s loop of PfALDO make the pocket much more hydrophobic than the pocket in hALDO-A. Also, the conformation of the 290s loop in PfALDO results in a more constricted pocket than in hALDO-A (Figure 6). Although the structures of hALDO-B and hALDO-C are not available, the conformations of the 290s loops in all three human aldolase isozymes are most likely very similar due to the following reasons: (i) Leu-291, deleted from the PfALDO sequence, is conserved in all three human aldolase isozymes, (ii) Lys-293 of hALDO-A, which confers the greatly increased basicity of the 290s loop pocket compared to PfALDO, is also conserved in hALDO-B and is an Arg in hALDO-C. On the basis of the topological and electrostatic differences between the 290s loop regions of PfALDO and hALDO-A, a smaller, more hydrophobic compound may be a lead for the design of a ligand that selectively binds this pocket in PfALDO.

The conformation of the 290s loop pocket as seen in PfALDO is likely representative of all *Plasmodium* aldolases. Indications for this come from the two other known *Plasmodium* aldolase sequences, both from the murine malaria parasite *P. berghei* (*32*), which show that the 290s loop is virtually identical in all three *Plasmodium* aldolases of known amino acid sequence. Residues 294−301 of one *P. berghei* aldolase are identical to those of PfALDO, and in the other *P. berghei* aldolase, the only amino acid difference from PfALDO in this region is Ala-295 in PfALDO going to Val in the murine malaria aldolase. Given the fact that the two *P. berghei* aldolases are 99% and 87% sequence-identical with PfALDO and likely representative of most if not all *Plasmodium* aldolases (*34*), the conformation of the loop spanning residues Asn-294−Trp-301 appears to be characteristic of malarial aldolases, like the Lys-Lys tandem of the C-terminal tail. Hence, compounds exploiting the difference in the 290s loop region between human and malarial aldolases might be useful for the treatment of all four variants of human malaria, caused by *Plasmodium* species *falciparum*, *vivax*, *malariae*, and *ovale*.

It is of interest that the 290s loop pocket is very close to the beginning of the C-terminal tail of the enzyme, as Gly-346 defines part of the 290s loop pocket. Comparison of the PfALDO and hALDO-A structures shows that their C-terminal tails begin to diverge at Lys-349 of PfALDO. Upon superposition, the C^{α} deviation between Tyr-348 of PfALDO and Tyr-342 of hALDO-A is 0.8 Å, while the C^{α} deviation between Lys-349 of PfALDO and Thr-343 of hALDO-A is 2.2 Å. It should therefore be possible to arrive at compounds that bind in the hydrophobic pocket and affect the mobility and positioning of the catalytically important C-terminal tail. However, given the length of the tail, it remains to be seen if interference with the conformation of Gly-346 through Lys-349 at the beginning of the PfALDO C-terminal tail will have major consequences for the catalytic efficiency, which is significantly affected by the C-terminal Tyr.

Another possible anti-PfALDO action of a compound binding in the 290s loop pocket is quaternary structure disruption. Even though the design of small molecules that interfere with the intersubunit interactions of oligomers is considered a very difficult goal to achieve, there are examples of successful interference of protein−protein interactions by small peptides, as in the case of ribonucleotide reductase (*35*) and the human estrogen receptor (*36*). In the aldolase tetramer, the 290s loop region is near the AD dimer interface. As mentioned earlier, there is 40% less buried surface area in the PfALDO AD interface compared with the hALDO-A AD interface. Part of this increased buried surface area in the hALDO-A AD dimer interface is due to differences between the conformations of the 290s loops in PfALDO and hALDO-A. In hALDO-A, Leu-292 contacts Pro-294 in the 290s loop of the AD dimer mate. Due to differences in the conformations of the 290s loop, Pro-298 in PfALDO,

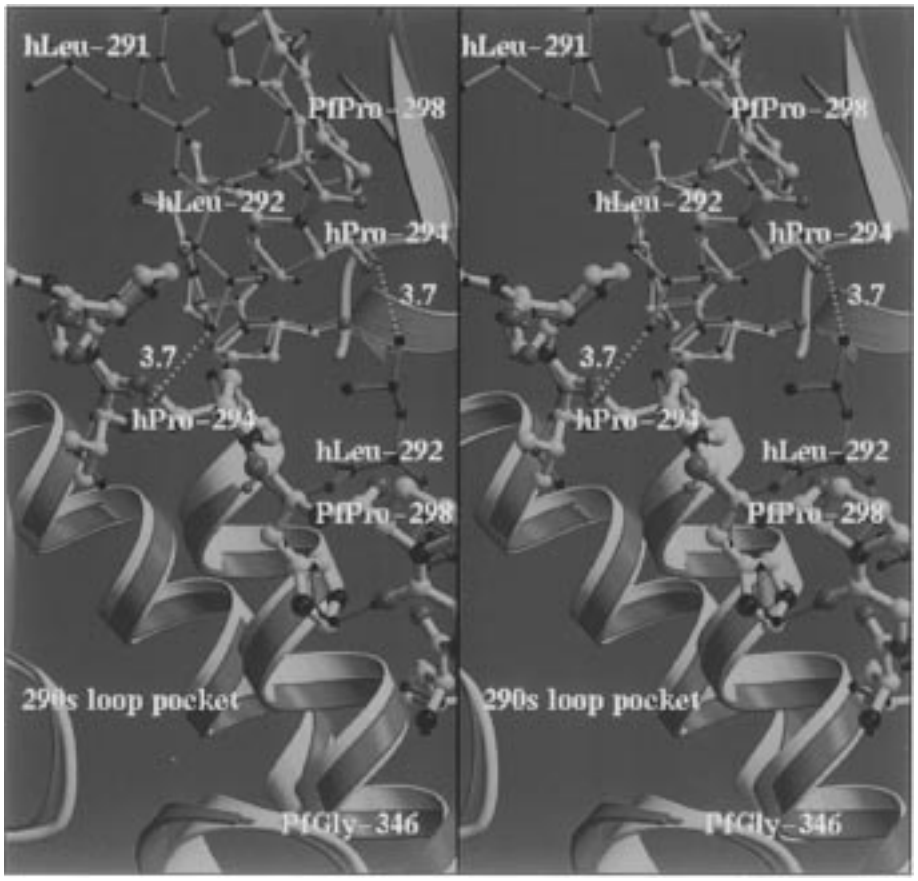

FIGURE 7: Stereoview of the AD−dimer interface at the 290s loop region. PfALDO and hALDO-A are shown after superposition of the entire hALDO-A tetramer onto the entire PfALDO tetramer. The A subunit of PfALDO is drawn with thick yellow ribbon and bonds, and the D subunit of PfALDO is drawn with thinner beige ribbon and bonds. The A subunit of hALDO-A is drawn with magenta ribbon and bonds, and the D subunit of hALDO-A is drawn with thinner pink ribbon and bonds. The 290s loop pocket is indicated. Distances between Leu-292 and Pro-294 of the dimer mate in hALDO-A are indicated by dashed lines and given in angstroms. Note the different courses of the backbones of the 290s loops in PfALDO [with PfPro-298 labeled) and hALDO-A [with the sequence-corresponding hLeu-292 labeled; see Figure 4 (right)]. The figure was made with MOLSCRIPT and RASTER3D (*47*).

the residue corresponding to Leu-292 in hALDO-A, is not involved in AD dimer contacts (Figure 7). Thus, a ligand that selectively bound in the PfALDO 290s loop region could serve as the basis for a compound that disrupts the AD dimer interface or even prevents it from forming.

The effect of quaternary structure disruption would probably be to reduce the thermostability of the PfALDO monomer. Although aldolase is not an allosteric enzyme, and its tetrameric structure is not required for enzymatic activity (*37*), disruption of the aldolase tetramer results in reduced thermostability. Studies on rabbit aldolase A have shown that both the melting temperature, T_m, and half-inactivation temperature, $T_{0.5}$, are decreased upon disruption of the tetramer into dimers and monomers. The aldolase tetramer is also more resistant to inactivation by urea than is the monomer (*38*).

Evidence for the importance of an intact aldolase tetramer *in vivo* has appeared in the medical literature. For example, hALDO-A deficiency is associated with hereditary hemolytic anemia (*39*). Analysis of one patient's hALDO-A cDNA revealed a single nucleotide substitution that led to the D128G mutant hALDO-A (*40*). Asp-128 occurs at the AB dimer interface in hALDO-A. This D128G mutant hALDO-A was thermolabile, and later it was shown by studies on rabbit aldolase A, which has the same dimer interface structure as hALDO-A, that this mutant existed as a mixture of dimers and tetramers at 4 °C and was more than 99% dimeric at 20 °C (*41*). Although the D128G rabbit aldolase was active, its T_m was lowered by 12 °C compared with the native hALDO-A, a factor likely contributing to the human genetic disease caused by the D128G mutation of hALDO-A.

These *in vitro* studies on quaternary structure disruption of rabbit aldolase and the human genetic diseases related to aldolase oligomerization suggest that interference with the quaternary structure of PfALDO could have serious consequences for *P. falciparum*. In the parasite, glycolysis proceeds at a tremendous rate. It has been proposed that the glycolytic enzymes are organized *in vivo* such that successive enzymes in the pathway are clustered together for efficient channeling of metabolites (*42*). Indeed, it has been shown that coimmobilized glycolytic enzymes are more efficient than the corresponding solubilized enzymes (*43*). Considering the rate of glycolysis in *P. falciparum*, it may be that the glycolytic enzymes of this parasite are grouped to increase their enzymatic efficiency. PfALDO has been shown to bind peptides derived from the malarial cytoskeletal proteins α-tubulin and actin II (*33*), and a grouped organization of glycolytic enzymes, including aldolase, has been proposed for *P. falciparum* (*12*). Thus, a small molecule that interferes with the oligomerization of PfALDO may not only lower the thermostability and activity of PfALDO but

also have a deleterious effect on a higher level multiprotein organization within the parasite. Such a strategy should be investigated further for antimalarial therapy.

ACKNOWLEDGMENT

We gratefully acknowledge Stewart Turley for maintaining our in-house data collection systems. We thank Henry Bellamy (SSRL), Richard Kahn (ESRF), Matthew Redinbo, Lance Stewart, and David Chudzik for assistance in synchrotron data collection.

REFERENCES

1. Butler, D. (1997) *Nature 386*, 535−536.
2. Sherman, I. W. (1984) *Antimalarial drugs*, Chapter 2: Metabolism, in *Handbook of Experimental Pharmacology 68/I* (Peters, W., and Richards, W. H. G., Eds.) pp 31−81. Springer-Verlag, Berlin.
3. Döbeli, H., Itin, C., Meier, B., and Certa, U. (1991) *Acta Leiden. 60*, 135−140.
4. Muirhead, H., and Watson, H. (1992) *Curr. Opin. Struct. Biol. 2*, 870−876.
5. Fothergill-Gilmore, L. A., and Michels, P. A. (1993) *Prog. Biophys. Mol. Biol. 59*, 105−235.
6. Penhoet, E. E., Kochman, M., and Rutter, W. J. (1969) *Biochemistry 8*, 4396−4402.
7. Yeltman, D. R., and Harris, B. G. (1977) *Biochim. Biophys. Acta 484*, 188−198.
8. Hester, G., Brenner-Holzach, O., Rossi, F. A., Struck-Donatz, M., Winterhalter, K. H., Smit, J. D. G., and Piontek, K. (1991) *FEBS Lett. 292*, 237−242.
9. Sygusch, J., Beaudry, D., and Allaire, M. (1987) *Proc. Natl. Acad. Sci. U.S.A. 84*, 7846−7850.
10. Millar, J. R., Shaw, P. J., Stammmers, D. K., and Watson, H. C. (1981) *Philos. Trans. R. Soc. London, B 293*, 209−214.
11. Gamblin, S. J., Cooper, B., Millar, J. R., Davies, G. J., Littlechild, J. A., and Watson, H. C. (1990) *FEBS Lett. 262*, 282−286.
12. Döbeli, H., Trzeciak, A., Gillessen, D., Matile, H., Srivastava, I. K., Perrin, L. H., Jakob, P. E., and Certa, U. (1990) *Mol. Biochem. Parasitol. 41*, 259−268.
13. Ghersa, P., Srivastava, I. K., Perrin, L. H., Döbeli, H., Becherer, D. J., Matile, H., Meier, B., and Certa, U. (1990) *EMBO J. 9*, 1645−1649.
14. Otwinowski, Z. (1993) in *Data Collection and Processing, Proceedings of the CCP4 Study Weekend* (Sawyer, L., Isaacs, N., and Bailey, S., Eds.) pp 56−62, SERC Daresbury Laboratory, Warrington, U.K.
15. Kabsch, W. (1988) *J. Appl. Crystallogr. 21*, 67−71.
16. Kabsch, W. (1988) *J. Appl. Crystallogr. 21*, 916−924.
17. Kabsch, W. (1993) *J. Appl. Crystallogr. 26*, 795−800.
18. Collaborative Computational Project No. 4. (1994) *Acta Crystallogr. D 50*, 760−763.
19. Read, R. J. (1986) *Acta Crystallogr. A 42*, 140−149.
20. Cowtan, K. (1994) Joint *CCP4 and ESF.−EACBM Newsletter on Protein Crystallography*, Vol. 31, pp 34−38, Daresbury Laboratories, Daresbury, U.K.
21. Brünger, A. T. (1992) *X-PLOR, Version 3.1: A System for X-ray Crystallography and NMR*, Yale University Press, New Haven, CT.
22. Jones, T. A., Zou, J.-Y., Cowan, S. W., and Kjeldgaard, M. (1991) *Acta Crystallogr. A 47*, 110−119.
23. Kleywegt, G. J., and Jones, T. A. (1996) *Structure 4*, 1395−1400.
24. Gefflaut, T., Blonski, C., Perie, J., and Willson, M. (1995) *Prog. Biophys. Mol. Biol. 63*, 301−340.
25. Blom, N., and Sygusch, J. (1997) *Nat. Struct. Biol. 4*, 36−39.
26. Drechsler, E. R., Boyer, P. D., and Kowalsky, A. G. (1959) *J. Biol. Chem. 234*, 2627−2634.
27. Rutter, W. J., Richards, O. C., and Woodfin, B. M. (1961) *J. Biol. Chem. 236*, 3193−3197.
28. Silva, A. M., Lee, A. Y., Gulnik, S. V., Majer, P., Collins, J., Bhat, T. N., Collins, P. J., Cachau, R. E., Luker, K. E., Gluzman, I. Y., Francis, S. E., Oksman, A., Goldberg, D. E., and Erickson, J. W. (1996) *Proc. Natl. Acad. Sci. U.S.A. 93*, 10034−10039.
29. Dunn, C. R., Banfield, M. J., Barker, J. J., Higham, C. W., Moreton, K. M., Turgut-Balik, D., Brady, R. L., and Holbrook, J. J. (1996) *Nat. Struct. Biol. 3*, 912−915.
30. Velanker, S. S., Ray, S. S., Gokhale, R. S., Suma, S., Balaram, H., Balaram, P., and Murthy, M. R. N. (1997) *Structure 5*, 751−761.
31. McKee, R. W. (1951) in *Biochemistry and Physiology of Protozoa*, S. H. (Hutter, S. H., and Lwoff, A., Eds.) Vol. 1, pp 251−322, (Academic Press, New York).
32. Meier, B., Döbeli, H., and Certa, U. (1992) *Mol. Biochem. Parasitol. 52*, 15−28.
33. Itin, C., Burki, Y., Certa, U., and Döbeli, H. (1993) *Mol. Biochem. Parasitol. 58*, 135−144.
34. Escalante, A. A., and Ayala, F. J. (1994) *Proc. Natl. Acad. Sci. U.S.A. 91*, 11373−11377.
35. Marcello, A., and Palu, G. (1995) *J. Chemother. 7*, 403−405.
36. Arnold, S. F., and Notides, A. C. (1995) *Proc. Natl. Acad. Sci. U.S.A. 92*, 7475−7479.
37. Chan, W. W.-C., and Mawer, H. M. (1972) *Arch. Biochem. Biophy. 149*, 136−145.
38. Beernink, P. T., and Tolan, D. R. (1996) *Proc. Natl. Acad. Sci. U.S.A. 93*, 5374−5379.
39. Miwa, S., Fujii, H., Tani, K., Takahashi, K., Takegawa, S., Fujinami, N., Sakurai, M., Kubo, M., Tanimoto, Y., Kato, T., and Matsumoto, N. (1981) *Am. J. Hematol. 11*, 425−437.
40. Kishi, H., Mukai, T., Hirono, A., Fujii, H., Miwa, S., and Hori, K. (1987) *Proc. Natl. Acad. Sci. U.S.A. 84*, 8623−8627.
41. Beernink, P. T., and Tolan, D. R. (1994) *Protein Sci. 3*, 1383--1391.
42. Masters, C. J., Reid, S., and Don, M. (1987) *Mol. Cell. Biochem. 76*, 3−14.
43. Luca, M. D., and Kricka, L. J. (1983) *Arch. Biochem. Biophys. 226*, 285−291.
44. Kraulis, P. J. (1991) *J. Appl. Crystallogr. 24*, 946−950.
45. Arnez, J. G. (1994) *J. Appl. Crystallogr. 27*, 649−653.
46. Nicholls, A., Sharp, K. A., and Honig, B. (1991) *Proteins: Struct., Funct., Genet. 11*, 281−293.
47. Merritt, E. A., and Murphy, M. E. P. (1994) *Acta Crystallogr. D 50*, 869−873.

BI972233H